

The MU2E project

M. Cordelli, S. Giovannella, F. Happacher, A. Luca (Laur.), S. Miscetti (Resp.),
A. Saputi (Tecn.), I. Sarra (Dott.), V. Stomaci (Laur.)

1 The Mu2e experiment

The Mu2e experiment, proposed at Fermilab, aims to search for the neutrinoless, coherent conversion of a negative muon into an electron in the Coulomb field of a nucleus ¹). The measurement will be expressed by the ratio of the muon-to-electron conversion rate relative to the ordinary muon capture rate on an aluminium nucleus:

$$R_{\mu e} = \frac{\Gamma(\mu^- + Al \rightarrow e^- + Al)}{\Gamma(\mu^- + Al \rightarrow \nu_\mu + Mg)}. \quad (1)$$

The process of muon to electron conversion is an example of Charged Lepton Flavor Violation (CLFV). While it is strongly suppressed in the Standard Model (SM), ($\text{BR}(\mu \rightarrow e) \approx 10^{-54}$), many scenarios of physics beyond the SM, predict enhanced BRs close to the reaches of current or near future experiments. Therefore, any signal is a compelling evidence of New Physics. If no events are seen in the signal window, the experiment is designed to set an upper limit of $R_{\mu e} \leq 6 \times 10^{-17}$ at 90% C.L. in three years of running. This value represents an improvement of four orders of magnitude over the current best experimental limit $R_{\mu e}(Au) < 7 \times 10^{-13}$, from the SINDRUM II experiment ²). The conversion of a muon to an electron in the field of a nucleus occurs coherently, resulting in a monoenergetic electron with an energy equal to the muon rest mass, apart from corrections for the nuclear recoil and the K-shell binding energy of the muon ($E_e = 104.97$ MeV). This distinctive signature has several experimental advantages, including the near-absence of background from accidentals and the suppression of background electrons near the conversion energy from muon decays. At the proposed Mu2e sensitivity, the most important background sources are: (1) intrinsic processes that include muon *Decay-In-Orbit* (or DIO) and radiative muon capture (RMC), (2) *delayed* processes due to particles that spiral slowly down the muon beamline, such as antiprotons, (3) prompt processes where a beam particle can arrive at the muon stopping target nearly coincident in time with the the detected electron, (4) electrons that are initiated by cosmic rays, (5) events that result from reconstruction errors in the detector.

Among the potential backgrounds, the muon *Decay-In-Orbit* is of particular concern, contributing about half the total background in the signal energy region. The process is $[\mu^- Al]_{bound}^{1s} \rightarrow e^- Al \nu_\mu \bar{\nu}_e$, with a bound muon which decays in orbit in aluminium and produces an electron that can mimic the signal: the outgoing electron recoils off the nucleus and will have exactly the conversion energy, in the limit that the neutrinos have zero energy. The bulk energy is below $m_\mu/2 \approx 52.8$ MeV, which corresponds to the Michel endpoint for free muon decay, and the nuclear recoil gives rise to a small tail that extends out to the conversion energy (Fig. 1). Since the DIO rate falls as $\approx (E_{conversion} - E)^5$ as the electron energy approaches the endpoint, this background can be overcome through adequate electron energy resolution.

The overall design of Mu2e is driven by the need to suppress potential backgrounds and to produce a high intensity, low energy muon beam that should provide around 10^{18} stopped muons on target. The desired Mu2e muon beam will be produced using the Fermilab accelerator complex, which will deliver 8 GeV protons into the *Mu2e beamline*. A pulsed structure of beam and a veto gate allow prompt beam background to die down during 750 ns, after which the detector is activated to look for μ -atom decays. The Mu2e beamline consists in an evacuated inner bore (to 10^{-4} Torr) of

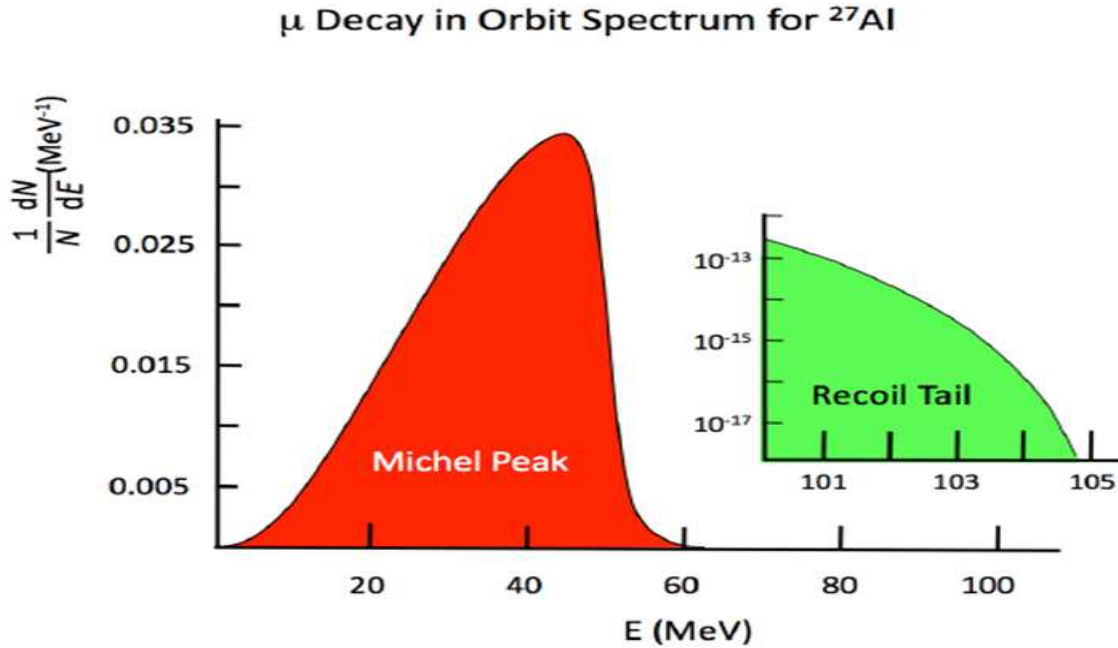


Figure 1: *The electron energy spectrum for muon decay in orbit in aluminum. The recoiling nucleus results in a small tail (blown up on the right) that extends out to the conversion energy.*

a series of superconducting solenoids which form a graded magnetic field: the Production Solenoid (PS), the Transport Solenoid (TS) and the Detector Solenoid (DS). The PS contains the production target that intercepts the proton beam. Pions produced by target interactions and the muons into which they decay are captured. The muon stopping target composed of a set of thin aluminium foils and has a graded magnetic field. The graded field increases the acceptance for conversion electrons and plays a key role in rejecting certain backgrounds. The downstream section of the DS has a nearly uniform field ($< 1\%$ non-uniformity) in the region occupied by the Tracker and the Calorimeter that accurately analyze electrons emerging from the stopping foils. The detector system must be cylindrical with a central hole where the remnant muon beam and most of the DIO electrons pass through (executing helices with small radii). Fig. 2 shows the muon beamline and the detector system. A description of the solenoidal systems and of the main backgrounds expected in the experiment can be found in Ref. ³).

The LNF group, together with INFN groups of Pisa and Udine is in charge of the construction of the calorimeter, EMC, with an assigned role of L2 management. An INFN group from Lecce is proposing an alternative system for the tracking based on a cylindrical drift chamber.

In this report, we show the design of the calorimeter, the results obtained at 100 MeV with a small size prototype and the excellent data-MC comparison for these data. We also show the simulation of the calorimeter in the Mu2e software framework and the plans for R&D and calibration.

During 2012, our group participated to many technical reviews at Fermilab and was in charge for the preparation of the CDR chapter on calorimetry, the cost estimate (BOE, WBS) and the schedule preparation. On June 2012, the CD-1 review meeting was successfully held. The experiment got CD-1 approval on July 11.

2 The Mu2e electromagnetic calorimeter

The calorimeter has to match a given set of requirements driven by the need of confirming that the candidates reconstructed by the extremely precise tracker system are indeed conversion electrons.

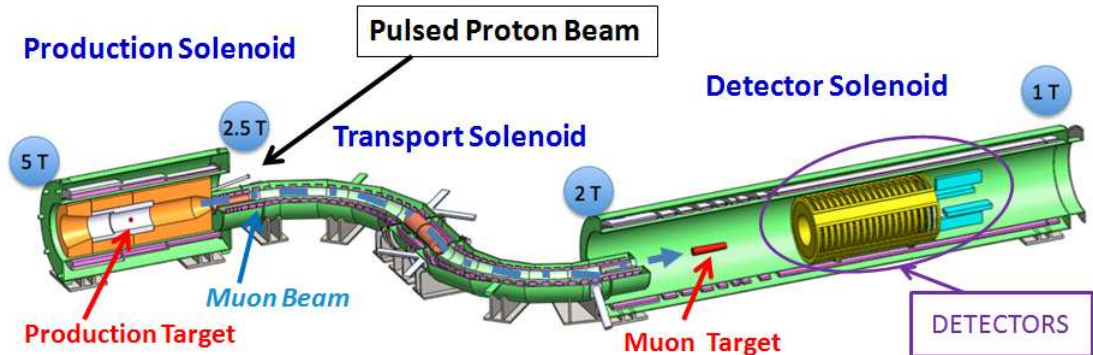


Figure 2: An overview of the Mu2e detector.

We therefore look for a calorimeter with a large acceptance for signal events, an excellent energy resolution $\mathcal{O}(2\%)$ and a reasonable position (time) resolution of few mm (< 1 ns) to compare the impact point (the arrival time) of the tracks on the calorimeter surface. Moreover, the calorimeter should also provide a trigger (or a reduction filter) for the experiment and be able to perform a powerful μ^-/e^- particle identification. Finally, it should be able to keep functionality in an environment where the n, p and γ background coming from muon capture processes and beam flash events deliver a dose of ~ 200 Gy/year in the hottest area. It will also need to work immersed in 1 T axial magnetic field and in a 10^{-4} torr vacuum enclosure inside the Detector Solenoid.

In order to achieve the required energy resolution at 100 MeV, a total absorption homogeneous calorimeter is needed. Among the potential materials for such a calorimeter we focused on two types of scintillating crystals: an improved version of the classical lead tungstate PbWO_4 which has been developed for the PANDA calorimeter⁴⁾ and the Cerium-doped Lutetium Yttrium Oxorthosilicate, LYSO. They both have certain desirable characteristics: they have fast scintillation decay times, similar Molière radii, reasonable mechanical properties and are not hygroscopic. There are differences, however: LYSO has a slightly lower density and a slightly longer radiation length, but has a light yield a factor of ~ 200 better than the PbWO_4 at room temperature. It is more radiation hard, and its scintillation light output has a much reduced dependence on temperature with respect to PbWO_4 crystals. The light emission spectrum of LYSO peaks at 402 nm, slightly lower than that of PbWO_4 , but both are compatible with APD readout. LYSO has been selected as the primary choice since the energy resolution terms will be dominated by leakage and intrinsic uniformity of the crystal. The noise and photostatistic term can be easily reduced to be negligible.

The proposed calorimeter consists of 1952 LYSO crystals located downstream of the tracker and arranged in four homogeneous parallelepiped vanes as shown in Fig. 3. The inner radius (36 to 39 cm) allows DIO electrons with $p_T > 55$ MeV to pass through the central hole, without registering a hit. Each vane is an array of 11×44 crystals, $(3 \times 3 \times 11)$ cm³ each, and will be equipped with two Avalanche Photodiodes (APDs) which work well in a magnetic field. The usage of two APDs per crystal increases the light yield, provides redundancy and allows for the correct energy to be determined if a charged particle passes through one of the APDs. APD signals are amplified and

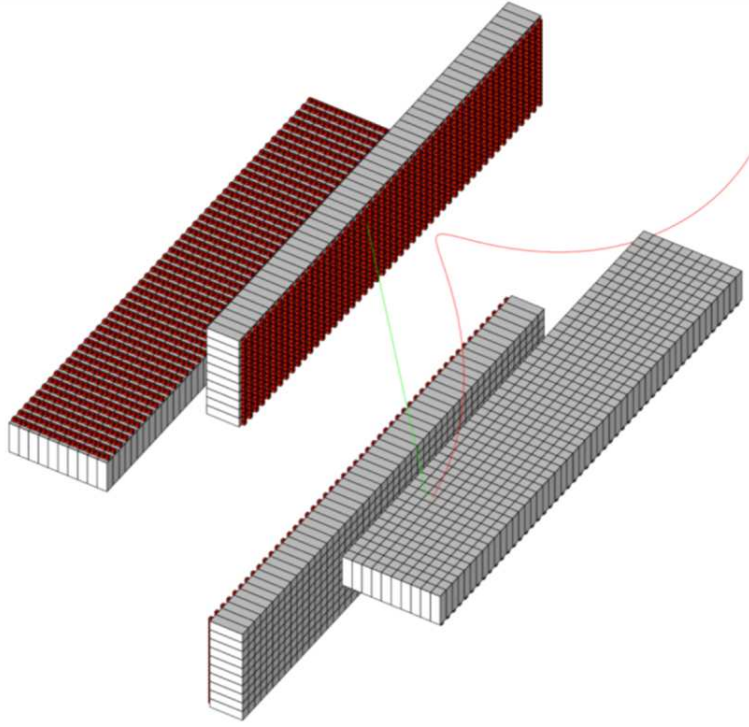


Figure 3: *The electromagnetic calorimeter is composed of four vanes. An electron, exhibiting a spiral path, hits the active face. The opposite face houses an APD based readout package.*

shaped and then readout through 200 MSPS waveform digitizers optically connected to the DAQ system. An alternative geometry that improves acceptance by using a disk-based geometry is also currently under evaluation.

An absolute calibration will be performed using a *source calibration system*. This system, successfully used in the BaBar experiment ⁵⁾, is based on an activated compound which produces the decay chain $^{19}\text{F} + n \rightarrow ^{16}\text{N} + \alpha$, $^{16}\text{N} \rightarrow ^{16}\text{O}^* + e^- + \nu_e$, $^{16}\text{O}^* \rightarrow ^{16}\text{O} + \gamma$. The resulting energy spectrum (see Fig. 4) has a peak corresponding to the 6.13 MeV photon line from $^{16}\text{O}^*$ and two escape peaks at 5.62 MeV, 5.11 MeV. Thus, such an approach can also provide a measurement of linearity. We plan to monitor, in a more continuous way than with the source, the variations of the crystal optical transmittance and of the APD gains by means of a laser system: blue and red light will be transported with optical fibers to the back of each LYSO crystal.

We have tested the EMC capabilities with a full simulation of signal and DIO background events in the Mu2e Framework software. One important achievement is obtained with a simple trigger algorithm that could be implemented in hardware to drastically reduce the bandwidth of DAQ system. This method just applies different threshold values to the reconstructed energy clusters and gives an efficiency of $\sim 91\%$ on signal events with a DIO reduction rate of a factor of 120 (i.e. 1.5 kHz maximum rate) with respect to tracker, at 64 MeV. This study is performed as a function of achievable calorimeter energy resolution (1, 1.5, 5 and 10 MeV), as shown in Fig. 5. We have developed a clustering method based on contiguity of fired cells. We have also developed a technique to reconstruct the impact point position along z. We get a resolution of about 1 mm for the Gaussian core (80% of the events) and 6 mm for the tails (20%). We have also studied the Pion Identification Capability of the calorimeter with respect to muons and electrons.

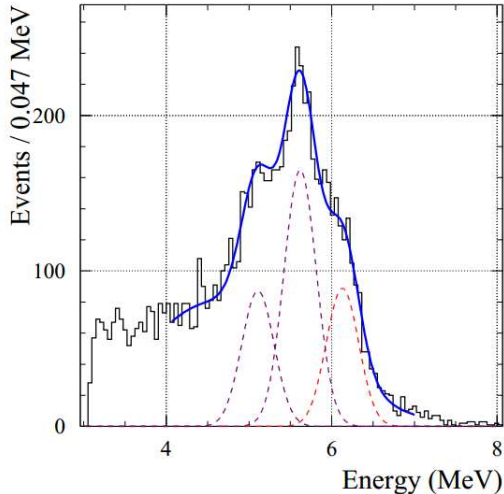


Figure 4: *Energy spectrum in a BaBar CsI(Tl) crystal irradiated with 6.13 MeV photons from an $^{16}O^*$ source.*

2.1 Test results with photon beams

We have tested a calorimeter prototype with a clean tagged photon beam at MAMI (Mainz Microtron) facility in Germany. The matrix prototype was built in February 2011, with transverse dimensions corresponding to $\sim 2.8 R_M$ and longitudinal dimensions of 13-15 cm ($\sim 11 \div 12 X_0$). The prototype consists of an inner matrix of 9 LYSO crystals by SICCAS ($2 \times 2 \times 15 \text{ cm}^3$) readout by APDs S8664 ($10 \times 10 \text{ mm}^2$ produced by Hamamatsu) and an outer matrix for leakage recovery, composed by 8 PbWO_4 crystal sectors (being constrained by budget), readout by standard Hamamatsu Bialcali photo multipliers of 1 inch of diameter. The realization of such a prototype has been a joint work with KLOE-2 Collaboration.

In the facility hall A2 the electron beam is converted to an intense beam of real photons through bremsstrahlung in a thin metal foil radiator. The scattered electrons in this process are momentum analyzed by plastic scintillator spectrometer which provides a determination of the energy of the associated bremsstrahlung photon with a resolution of few per mil. The tagged photon beam is excellent, having $\Delta p(\text{FWHM}) = 1 \text{ MeV}$ and a cross section on the calorimeter front face of about 8 mm diameter. The calorimeter prototype was installed over a movable table allowed to adjust the position of the matrix with respect to the photon beam.

We have triggered by using a coincidence between the OR signal from the inner matrix and the signal from the beam tagging system. We acquired data with a CAMAC system, reading out LeCroy ADC and TDC boards with a sensitivity of 250 fC/count and 100 ps/count, respectively. The data acquisition was writing on disk at $\sim 10 \text{ Hz}$. The temperature of the experimental hall ($\sim 24 \text{ }^\circ\text{C}$) was continuously monitored with thermo-sensors attached to the electronics and preamplifiers and was stable at the level of $\pm 0.5^\circ\text{C}$.

The FEE has been developed by a collaboration of Laboratori Nazionali of Frascati and Roma 2 University. This consists in an amplifier first stage, composed by a MAR8A + discrete amplifier by Microcircuits with a gain of ~ 20 , and second stage buffer, made of a LMH6559 high-speed buffer by National Semiconductor. In order to minimize the gain variation we have also developed a new High Voltage board. This shows a stability of 20-30 mV, corresponding to $\delta G/G \sim 1\%$. Moreover it can be remotely adjusted and monitored with a sensibility of 30 mV.

We have taken data in March 2011 with the photon beam (100-500 MeV) impinging at the center of the inner crystal matrix. The same photon energy (100 MeV) was used for the position dependence scan. Pedestal and test pulse runs were performed once every few hours during the

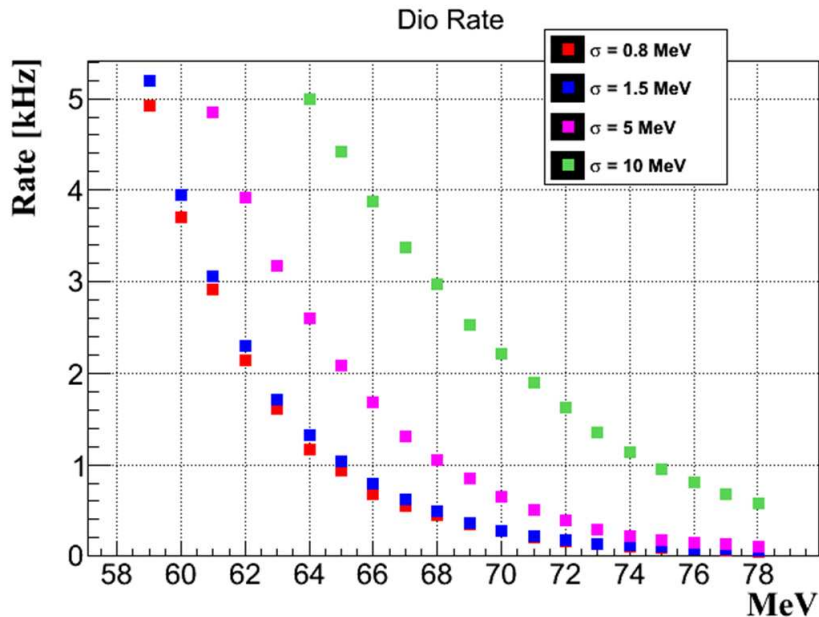


Figure 5: *DIO* rate on fiducial calorimeter faces as a function of energy thresholds, for different energy resolution values.

beam time to check the system stability. Cosmic Rays (CR) were used for the calibration. We took CR calibration data during the off-beam periods by means of an external trigger provided by a coincidence of a pair of scintillator counters. We have calibrated the calorimeter response of each channel with minimum ionizing particles (MIPs), crossing the calorimeter orthogonally to the crystal axis. The energy scale has been set looking at the linearity in response with the photon beam, and is set to 18.8 MeV per MIP consistently with average LYSO number. We get σ_{ped} of 3 (2) counts and a MIP peak around 120 (250) counts for the inner (external) crystals. The statistical precision on the peak determination is $\sim 2\%$.

The total response of the detector is defined as $Q_{TOT} = \sum_i (Q_i - P_i) \cdot 1/M_i$, where Q_i and P_i are the collected charge and the pedestal of the i -th channel and M_i is the minimum ionization peak. To understand the different terms contributing to the energy resolution, we have carried out a full simulation of the prototype based on Geant-4. Fig. 6 left shows a comparison between experimental data (black circles) and MC results (red distributions), for the energy deposit in the whole matrix, normalized to the beam energy at 100 MeV. We added a 4% Gaussian smearing for each channel in MC to reproduce data, obtaining a good data-MC agreement.

We have selected different beam energy values and fitted the corresponding energy distributions with a logarithmic Gaussian function⁶⁾, in order to quote the energy response and resolution. In Fig. 6 right, we show the energy dependence of the energy resolution which has been fitted with the following equation:

$$\sigma_E/E = a/\sqrt[4]{E[\text{GeV}]} \oplus b/E[\text{GeV}] \oplus c. \quad (2)$$

For experimental data, we found the stochastic term, a , to be $2.1 \pm 0.1\%$ and the constant term, c , to be $3.6 \pm 0.3\%$. The noise term b is practically negligible. The observed energy resolution (black points) well agrees with the expected one from MC with the 4% additional smearing (red points). Pink points refer to MC results without the degradation, which is believed to be due to the large variation in longitudinal uniformity. Longitudinal uniformity is an important specification for meeting the overall energy resolution goals. The calorimeter group has devised a method (involving

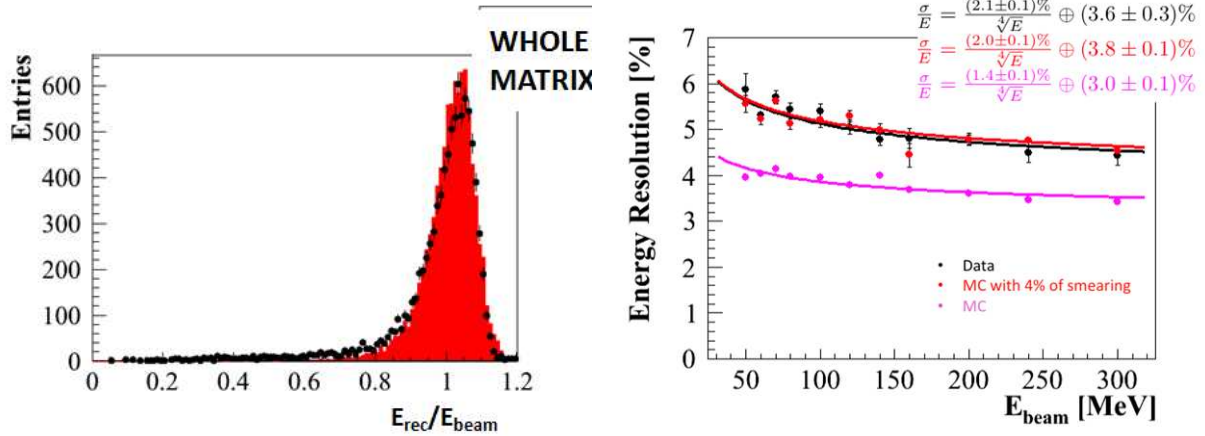


Figure 6: *Left: data (black) MC (red) comparison of energy deposit sum in the whole matrix, normalized to the beam energy, at 100 MeV. Right: data-MC comparison of the energy resolution as a function of beam momentum. Black points are data, red (pink) points are MC expectations with (without) the 4% correction.*

roughening one surface) to improve longitudinal uniformity by means of diffuse reflection. The crystals will be treated in this manner and re-exposed to a test beam prior to CD-2 to validate the anticipated energy resolution.

3 R&D and plans

One of the most crucial job for next year is to carry out simulation in the experiment and participating to the code development for a final version of the hit and cluster reconstruction. Moreover, we are carrying out R&D on many points:

1. measurement of the longitudinal response uniformity of the crystals;
2. measurement and choice of the photosensors ;
3. realization of the FEE and design of the digitizer algorithm;
4. calibration system based on the laser;
5. mechanical support.

We expect that during 2013 we will conclude the R&D for the crystals and photosensors and prepare a solid QC (Quality Control) specification for the crystal large size production. Engineering design of the QC station will be prepared. Prototypes of FEE amplification and HV regulation boards will be done. The goal is to get R&D completed for spring 2014, in order to successfully complete the CD-2 review.

The other basic milestone we are facing, it is that of completing another set of test beams with a larger size matrix and better FEE and system stability. We aim to reach experimental proof of getting an energy resolution of 2-2.5% at 100 MeV.

Acknowledgments

The authors are grateful to many people for the successful realization of the matrix. In particular, we thank all the LNF mechanical shop for the realization of the support and APD boxes, especially G. Bisogni, U. Martini and A. De Paolis. We thank B. Ponzio for the realization of the HV board and G. Pileggi for the help on the mechanical support of the matrix. We also thank the MAMI staff for providing the beam time. The realization of the preamplifiers was done in collaboration with E. Reali from Roma-2 University.

4 List of Conference Talks by LNF Authors in Year 2012

1. A. Lucà, “**The calorimeter project for the Mu2e experiment**”, 12th Pisa Meeting on Advanced Detectors, 20-26 May 2012, La Biodola, Isola d’Elba, Italy
2. I. Sarra, “**Test and Simulation of a LYSO+APD matrix with a tagged photon beam from 40 to 300 MeV**”, XVth International Conference on Calorimetry in High Energy Physics (CALOR2012), 48 June 2012, Santa Fe, USA

5 List of Papers/Proceedings

1. The Mu2e project and Collaboration, “**Mu2e Conceptual Design Report**”, <http://arxiv.org/abs/1211.7019>
2. J. Budagov *et al.*, “**The calorimeter project for the Mu2e experiment**”, <http://dx.doi.org/10.1016/j.nima.2012.11.177>
3. M. Cordelli *et al.*, “**Test and Simulation of a LYSO+APD matrix with a tagged photon beam from 40 to 300 MeV**”, J. Phys. Conf. Ser. **404** 012027 (2012)

References

1. The Mu2e Collaboration, R. M. Carey *et al.*, <http://mu2e-docdb.fnal.gov>, document 388-v1.
2. W. Bertl *et al.*, Eur. Phys. J. C **47**, 337 (2006).
3. The Mu2e Collaboration, R. J. Abrams *et al.*, <http://arxiv.org/abs/1211.7019>.
4. M. Kavatsyuk *et al.*, Nucl. Instr. Meth. A **648**, 77-91 (2011).
5. B. Aubert *et al.*, Nucl. Instr. Meth. A **479**, 1 (2002).
6. H. Ikeda *et al.*, Nucl. Instr. Meth. A **441** 401-426 (2000).
7. M. Cordelli *et al.*, Nucl. Instr. Meth. A **671** 109-112 (2010).